

# Fundamental parameters of two O9-type giant stars: the (former) spectral classification standard HD 93249 A and ALS 12502 A

T. Ansín<sup>1,2</sup> \*R. Gamen<sup>2,1</sup>, N. I. Morrell<sup>3</sup>, R. H. Barbá†, J. Maíz Apellániz<sup>4</sup>, J. I. Arias<sup>5</sup>, S. Simón-Díaz<sup>6,7</sup>, and G. Holgado<sup>4</sup>

<sup>1</sup>*Facultad de Ciencias Astronómicas y Geofísicas, Universidad Nacional de La Plata. Paseo del Bosque s/n, 1900, Argentina.*

<sup>2</sup>*Instituto de Astrofísica de La Plata, CONICET–UNLP. Argentina.*

<sup>3</sup>*Las Campanas Observatory, Carnegie Observatories. Casilla 601. La Serena, Chile.*

<sup>4</sup>*Centro de Astrobiología (CAB), CSIC-INTA. Campus ESAC. C. bajo del castillo s/n. E-28692 Madrid, Spain.*

<sup>5</sup>*Departamento de Astronomía, Universidad de La Serena. Cisternas 1200 Norte. La Serena, Chile.*

<sup>6</sup>*Universidad de La Laguna, Dpto. Astrofísica, E-38206 La Laguna, Tenerife, Spain.*

<sup>7</sup>*Instituto de Astrofísica de Canarias, Avenida Vía Láctea, E-38205 La Laguna, Tenerife, Spain.*

Received XXX; accepted XXX

## ABSTRACT

The evolution of massive stars is not completely understood. Several phenomena affect their birth, life, and death, multiplicity being one of them. In this context, the OWN and MONOS projects are systematically observing O- and WN-type stars whose multiplicity status is unknown. Their major goal considers the necessity of determining absolute parameters of massive stars. We have collected spectra of HD 93249 A and ALS 12502 A aiming at characterising their binary nature. For both stars, we analysed high-resolution spectra and combined them with *TESS* observations to be compared with binary models constructed by means of the *PHOEBE* code. We discovered that the radial velocity of HD 93249 A varies with a period of  $2.97968 \pm 0.00001$  d and that the system presents ellipsoidal light variations. We disentangled the composite spectra and classified its components as O9 III and B1.5 III, respectively. Confirmed as a spectroscopic binary, HD 93249 A can no longer be used as spectral classification standard. ALS 12502 A turned out to be a detached eclipsing binary in the *TESS* and *Gaia* data. These results enable us to determine absolute parameters for each component in the system.

**Key words:** binaries: spectroscopic – stars: early-type – stars: fundamental parameters – stars: individual (HD 93249 A) – stars: individual (ALS 12502 A)

## 1 INTRODUCTION

Determining the fundamental parameters of Galactic binary O-type stars is an arduous but very necessary task. Their scarceness is due to the relatively low number of O-type stars (there are only 611 entries in the Galactic O-Star Catalog (GOSC); Maíz Apellániz et al. 2013) and also to observational and instrumental issues which make difficult to reach reliable determinations. Among these difficulties we highlight the limited access to telescope time and the presence of some phenomena, such as pulsations or stellar wind inhomogeneities, which contaminate the stellar spectra and can mimic radial velocity variations. During the last two decades several efforts were carried out to discover new massive systems which allow determining the fundamental parameters of their components. There are a hundred of spectroscopic binary systems with O-type components and only a small percentage of them has well-determined absolute orbital parameters, i.e. the inclination is known. Moreover, only five binary systems with main-sequence O-type components have stellar parameters determined with uncertainties in  $L$  smaller than 30 %, and in  $R$  and  $M$  smaller than 3 % (Eker et al. 2015).

Discovering new binary systems is one of the major goals of the OWN survey, which since 2006 is monitoring with high resolution spectroscopy O- and WN-type stars observable from the Southern Hemisphere with multiplicity status unknown at the time of the beginning of the project (Gamen et al. 2008; Barbá et al. 2017). A parallel effort is being carried out in the Northern Hemisphere with the MONOS project (Maíz Apellániz et al. 2019b; Trigueros Páez et al. 2021), which is based on the LiLiMaRlin spectral library of libraries (Maíz Apellániz et al. 2019a) built from archival data and other projects such as IACOB (Simón-Díaz et al. 2011a; Simón-Díaz et al. 2015a, 2020), CAFÉ-BEANS (Negueruela et al. 2015), and NoMaDS (Pellerin et al. 2012). Newly discovered massive binary systems are analysed in detail with the objective of determining the elusive absolute masses, and other fundamental stellar parameters, such as radii and luminosities.

Due to our limited knowledge of massive star evolution, significant challenges remain in understanding the role of binarity/multiplicity and mass loss. To address this, we will focus on binary systems composed of O-type giants and subgiants, which are stars born with masses in the range  $\sim 15\text{--}80 M_{\odot}$  in an intermediate stage of their main sequence evolution. Furthermore, there is a noticeable dearth of giant and subgiant stars with precisely determined stellar parameters falling within the expected range of O9-type (cf.

\* Contact e-mail: tansin@fcaglp.unlp.edu.ar

† In memoriam (1962–2021)

the spectroscopic HR diagram, figure 11, in [Holgado et al. 2018](#), around  $T_{\text{eff}} \sim 33\,000$  K and  $\mathcal{L}/\mathcal{L}_{\odot} \sim 3.5$ , where  $\mathcal{L} := T_{\text{eff}}^4/g$ .

The Galactic O-Star Spectroscopic Survey (GOSSS, [Maíz Apellániz et al. 2011](#)) has been providing spectral classifications for O stars in the last decade. As of GOSSS III ([Maíz Apellániz et al. 2016](#)), there were ten stars catalogued as O9 III but only three of them were well known double-lined spectroscopic binaries (SB2), namely  $\iota$  Ori Aa,Ab (HD 37 043 Aa,Ab), ALS 12502 A (LS III +58 38 A), and HD 193 443 A,B (ALS 11 137 A,B). Subsequently, STIS has been used to spatially separate the two visual components in  $\iota$  Ori Aa,Ab and in HD 193 443 A,B ([Maíz Apellániz & Barbá 2020](#)). In the first case,  $\iota$  Ori Aa has been partially separated in velocity to yield a spectral type for its primary of O8.5 III (its secondary is only partially resolved while  $\iota$  Ori Ab spectral type is B2: IV:) while in the second case, HD 193 443 A is classified as O8.5 III(f) and HD 193 443 B is classified as O9.2 IV. These examples illustrate the difficulties of producing spectral classifications for O stars: some are like Matryoshkas (Russian dolls), with binaries hidden inside other binaries.

HD 93249 A ( $\alpha = 10^{\text{h}} 44^{\text{m}} 43.9^{\text{s}}$ ,  $\delta = -59^{\circ} 21' 25''$ , J2000.0) was first classified as O9 III by [Walborn \(1973\)](#). This classification was confirmed by GOSSS II ([Sota et al. 2014](#)), who pointed out to the double-lined binary nature (SB2) of this system based on information provided by the OWN survey, although the system was not kinematically resolved in GOSSS data. Given that lack of intermediate-resolution spectroscopy with double lines, GOSSS III ([Maíz Apellániz et al. 2016](#)) maintained HD 93249 A as the primary spectral classification standard of the subtype O9 III. HD 93249 A is the brightest early-type star in Trumpler 15 (Villafranca O-027), a stellar cluster in the Carina OB1 association at a distance of  $2355^{+61}_{-58}$  pc determined from *Gaia* DR3 parallaxes ([Molina-Lera et al. in preparation](#)). A similar distance,  $d=2.36\pm 0.09$  kpc, was found by [Shull et al. \(2021\)](#).

ALS 12502 A ( $\alpha = 22^{\text{h}} 34^{\text{m}} 46.0^{\text{s}}$ ,  $\delta = 58^{\circ} 18' 04''$ , J2000.0) was identified as an eclipsing binary system by [Maciejewski et al. \(2004\)](#) and as a SB2 by [Negeruela et al. \(2004\)](#). [Maíz Apellániz et al. \(2019b\)](#) found a third component in the spectrum, which likely corresponds to a source detected at 1.6 arcsec in AstraLux imaging. There are no spectrophotometric analyses in the literature.

Here we present our spectrophotometric analysis of the massive binary systems HD 93249 A and ALS 12502 A. The paper is organised as follows: the spectroscopic and photometric data are described in Sec. 2; the results of their analysis (Sec. 3) are split in several subsections as follows: the radial velocity (RV) measurements and disentangling are explained in Sec. 3.1, the new orbital solutions are shown in Sec. 3.2, and the spectrophotometric analysis are presented in Sec. 3.4; the fundamental parameters of the systems components are discussed in Sec. 4 and our conclusions are presented in Sec. 5.

## 2 OBSERVATIONAL DATA

### 2.1 Spectroscopic data

Thirty-four high-resolution spectra of HD 93249 A were collected during several observing runs between 2008 and 2019. We employed the échelle spectrographs attached to the 2-m class telescopes in Argentina and Chile, namely Jorge Sahade, CASLEO, Argentina; Irenée du Pont, Las Campanas Observatory (LCO), Chile; and MPG/ESO 2.2-m, La Silla (LS/ESO), Chile.

Fourteen LiLiMaRlin high-resolution spectroscopic epochs of ALS 12502 A were obtained between 2012 and 2022 with the

**Table 1.** Details of the instrumental configurations used in this work. The horizontal line divides the data for the two stars

Observatory/Telescope/Spectrograph	$\Delta\lambda$ [nm]	$R$	$n$
CASLEO/J. Sahade/REOSC-échelle	360–610	15 000	18
La Silla/2p2/FEROS	357–921	46 000	11
Las Campanas/I. du Pont/échelle	350–985	40 000	5
ORM/NOT/FIES	370–898	25 000	6
CAHA/CA-2.2/CAFE 2.2	393–922	65 000	5
ORM/Mercator/HERMES	380–900	85 000	3
Gemini/North/GRACES	410–1040	40 000	1

CAFÉ spectrograph at the 2.2 m Calar Alto telescope, Spain; HERMES at the 1.2 m Mercator Telescope; and FIES at the 2.6 Nordic Optical Telescope, the latter two at the Observatorio del Roque de los Muchachos, Spain. In addition, one spectrum was obtained with the Gemini Remote Access to CFHT ESPaDOnS Spectrograph (GRACES) during poor weather time (proposal: GN-2022B-Q-406), using the two-fiber configuration.

The instrumental configurations are described in Table 1, where in successive columns we give the observatory, telescope and spectrograph identification, the wavelength coverage ( $\Delta\lambda$ ), the spectral resolving power ( $R$ ), and the number of spectra collected ( $n$ ).

Data from CASLEO and LCO were processed and calibrated using standard IRAF<sup>1</sup> routines contained in the CCDPROC and ECHELLE packages. La Silla observations were reduced via the FEROS pipeline supported by ESO. The LiLiMaRlin spectra were reduced using the pipelines for those projects. The Gemini spectrum was processed by the CFHT OPERA open source pipeline.

### 2.2 Photometric data

#### 2.2.1 TESS

The Transiting Exoplanet Survey Satellite (*TESS*) has observed both stars. We found three sectors, 10, 36 and 37, containing photometric data of HD 93249 A, and 16, 17 and 24 with data of ALS 12502 A. Sector 10, 16 and 17 were visited during 2019, sector 24 during 2020, and sectors 36 and 37, during 2021. Exposure times were 1426 s (sector 10, 16, 17 and 24) and 475 s (sectors 36 and 37).

We downloaded cutouts of 15x15 pixels and performed aperture photometry on them using the LIGHTKURVE<sup>2</sup> v.2.0 ([Lightkurve Collaboration et al. 2018](#)) code within PYTHON package. We removed the background using the REGRESSIONCORRECTOR method included in the same package.

The chosen aperture for HD 93249 A includes the stars HD 93 249 B (= CPD –58 2659 B, B0.2 V(n) ([Berlanas et al. 2023](#))) and HD 93 249 C (= ALS 15 854, B1.5 V(n) ([Berlanas et al. 2023](#))), which are located at  $\sim 8''$  and  $\sim 9''$  from HD 93249 A, respectively (see Fig. 1). In the case of ALS 12502 A, we identified as contributors the component at  $1.6''$  ([Maíz Apellániz et al. 2019b](#)) and

<sup>1</sup> IRAF was distributed by the National Optical Astronomy Observatories which are operated by the Association of Universities for Research in Astronomy, under collaborative agreement with the US National Science Foundation.

<sup>2</sup> Lightkurve was built on top of a number of powerful libraries, including NumPy, SciPy, and Matplotlib ([Astropy Collaboration et al. 2013, 2018; Ginsburg et al. 2019; Brasseur et al. 2019](#)).

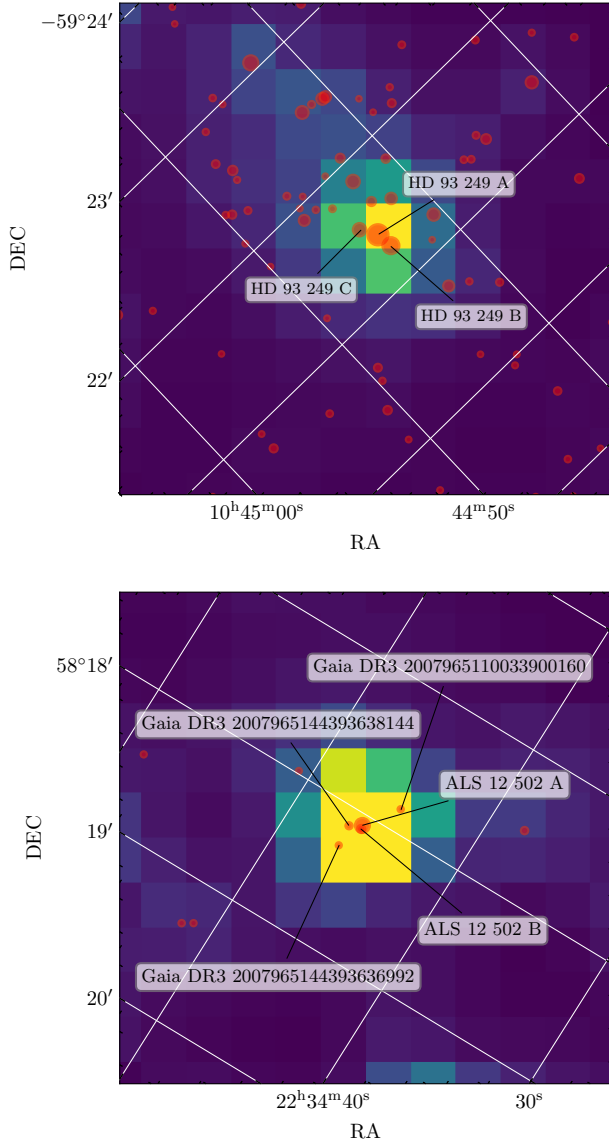


**Figure 1.** TESS pixel file of HD 93249 A (top panel) and ALS 12502 A (bottom), indicating the other stars considered as third light in the generated light curve.

four faint sources identified by *Gaia*. The contributions of these stars were considered as a constant third light in the spectrophotometric analysis of each system because no significant periods other than those due to orbital motion were found in the frequency analysis.

### 2.2.2 *Gaia*

As previously mentioned, the distance to Trumpler 15, the cluster to which HD 93249 A belongs, has been accurately measured as part of the Villafranca catalog of OB groups (Maíz Apellániz et al. 2020b, 2022). On the other hand, ALS 12502 A has good-quality *Gaia* DR2 + EDR3 photometry but poor-quality astrometry (a RUWE of 9.78 and a negative parallax), so an accurate individual distance cannot be determined from its *Gaia* EDR3 parallax. In order to determine the distance to ALS 12502 A, we use the same technique as in Maíz Apellániz et al. (2022) to obtain the properties (including distance) to its underlying cluster. That requires down-

loading the data for the *Gaia* EDR3 stars in the region and selecting the cluster members based on a combination of position, proper motions, and position in the CMD information, with a final cut in normalized parallax (see the two papers above for details). The cluster itself had been previously ignored in the literature and here we give it the Villafranca O-034 identifier and add it to the Villafranca catalog. Details on how we calculated the distance to Villafranca O-034 are given in Appendix B.

To determine the extinction towards HD 93249 A and ALS 12502 A we downloaded their *Gaia* DR2 + EDR3 and 2MASS photometry and processed it through CHORIZOS (Maíz Apellániz 2004). We followed a technique analogous to the one by Maíz Apellániz & Barbá (2018) and Maíz Apellániz et al. (2021a), also using the Maíz Apellániz (2013b) SED grid and the Maíz Apellániz et al. (2014) family of extinction laws. The details of the procedure are given in Appendix C.

The *Gaia* DR3 database also provides multi-epoch photometry of ALS 12502 A in the  $G$ ,  $G_{BP}$ , and  $G_{RP}$  bands.

## 3 RESULTS

### 3.1 Radial velocity determination and spectral analysis

The binary nature of HD 93249 A was inferred since the first observing runs of the OWN Survey, in 2008. We determined a preliminary SB2 orbit from the RVs of both components of the He I  $\lambda 5876$  absorption line using the NGAUSS task within IRAF. These results were published in Ansín et al. (2020).

We took advantage of those RV measurements to disentangle both spectra. To do this, we employed the 16 spectra obtained at La Silla and Las Campanas observatories, because they have higher resolution and SNR than CASLEO data. We shifted the spectra by the respective RVs of the primary component and combined them, obtaining an almost pure spectrum of the primary component as the spectral features of the secondary lied at different wavelengths and were diluted in the procedure, in addition to their intrinsic weakness (see Fig. 2). After that, we subtracted the obtained (almost) pure spectrum of the primary component from the composite spectra (RV-corrected) and the remaining spectra were combined, after shifted by the respective RVs of the secondary component. This way we should obtain the almost pure spectrum of the secondary star, but the results were not satisfactory (see below). The disentangling procedure is based on the method of González & Levato (2006) which was applied to other massive binary systems (see e.g. Gamen et al. 2015; Putkuri et al. 2018; Barbá et al. 2020; Putkuri et al. 2021). The method implies not only disentangling the spectra but also measuring the RVs of each component. This is performed using the FXCOR task within IRAF, which calculates the relative velocity between one of the templates and each composite spectrum from which the other template was subtracted. Each iteration produces new (more accurate) RVs which are used in the next combination. In the case of HD 93249 A the contribution of each component to the total flux is extremely different (see Fig. 2), and therefore the disentangling method leaves residuals from the primary spectrum in the secondary component's template which are similar in intensity to the secondary lines, seriously contaminating the secondary template. After several attempts, we found that we could obtain the spectrum of the secondary component using the IRAF task TELLURIC with the primary spectrum shifted in RV as template. After some iterations, the RVs do not change anymore and hence, the obtained templates either. The resulted disentangled spectra were good enough to con-

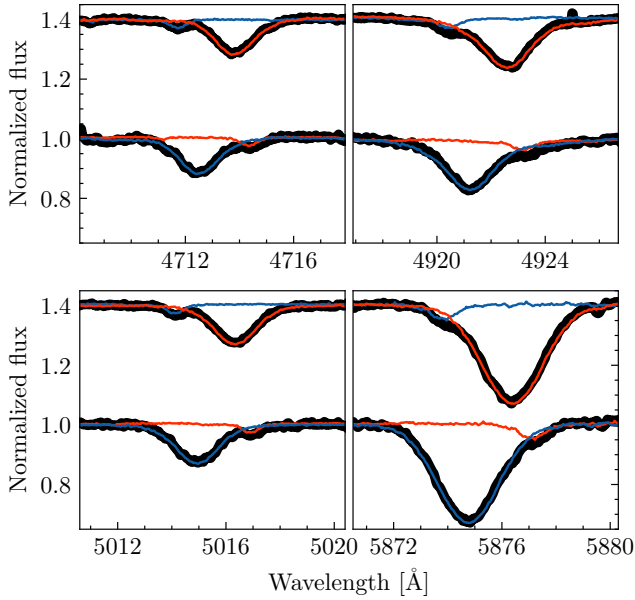


**Figure 2.** The composite spectrum of HD 93249 A at opposite quadratures, to show how the He I lines from both components compare to each other. Disentangled spectra for each component are superposed in colour.

continue our analysis. However, it should be pointed out that the disentangling process often leaves residuals affecting the profiles of the Balmer lines. We, therefore, avoided using Balmer lines as, for example, luminosity indicators for the HD 93249 A components.

Once a star is confirmed to be a spectroscopic binary, we can no longer use it as a classification standard. We then classified the primary component of HD 93249 A by comparison of its spectrum with those of HD 114 737 and HD 16 832 (see Fig. 3), which are the O8.5 III and O9.2 III classification standards in the temperature sequence, respectively (Maíz Apellániz et al. 2016). To determine its luminosity class, we compared the primary spectrum to HD 71 304 and HD 93 028, the O9 II and O9 IV classification standards (see Fig. 3). By interpolation between the adjacent categories, we confirm that HD 93249 Aa belongs to the O9 III spectral type. Its companion is very faint and does not contribute much to the composite spectrum (less than ten percent, see Section 4).

We found that the secondary spectrum is of type B, according to the criteria described in Walborn & Fitzpatrick (1990). We determined the ratio between Si III  $\lambda$ 4552 and Si IV  $\lambda$ 4089 and between Si II  $\lambda$ 4128–4130/Si III  $\lambda$ 4552. As the former is larger than the unity and no Si II  $\lambda$ 4128–4130 is detected, we concluded that the spectral type is between B0.5 and B2.5. In this range, C III + O II blends at  $\lambda$ 4070 and 4650 are the main criteria. Considering the intensities of Si III  $\lambda$ 4552 and He I  $\lambda$ 4388, which constitute the main criterion for the luminosity class, we classified HD 93249 Ab as B1.5 III. Fig. 4 compares the spectrum of HD 93249 Ab and the B1.5 III star 12 Lac.

Once the spectral characteristics of both components were known, we decided to use the RVs of He II  $\lambda$ 4542, 4686 and 5412 absorption lines as representative of the motion of the O9 III primary component and the RVs of He I  $\lambda$ 4713, 4922, 5016, and 5876, for the secondary B1.5 III component. The RV measurements were performed via the FXCOR task (within IRAF). We used the templates obtained as comparison and performed the cross-correlations over the composite spectra for the primary component and over the disentangled spectra for the secondary. The RVs determined by both methods (NGAUSS and FXCOR) are shown in Table A1.

**Table 2.** Rest (air) wavelengths for the lines used for RV measurements.

Line	Å	Line	Å
He II 4542	4541.591	He I 4713	4713.146
He II 4686	4685.682	He I 4922	4921.931
He II 5412	5411.524	He I 5016	5015.678
		He I 5876	5875.623

ALS 12502 A is a known SB2 (Negueruela et al. 2004) but has no RV orbit determined yet. We did not apply the disentangling method to this target as the spectral classification of both components was discussed by Maíz Apellániz et al. (2019b), who derived a classification of O9 IV(n) + O9 V(n), and besides features are well separated in most spectra because they were obtained during quadrature times (see Fig. 5). Thus, we measured the following absorption lines: He I  $\lambda$ 5876, He II  $\lambda$ 4686 and He II  $\lambda$ 5412, fitting simultaneously two Gaussian functions to each composite profile. We fixed the amplitude and width of each Gaussian function to the values found in the best separated spectrum, letting just fit the central wavelength. We used the facilities provided by the PYTHON SciPY environment. We finally averaged the results for the three lines (because their measurements are similar) to represent the stellar orbital motion of each component. The RVs determined are shown in Table A2.

### 3.2 New orbital solutions

The RVs presented in Tables A1 and A2 were used in the determination of orbital parameters for HD 93249 A and ALS 12502 A, respectively. The data were statistically weighted as follows: In the case of HD 93249 A, LCO and ESO spectra were weighted with unity and half weight was assigned to CASLEO data. For ALS 12502 A all data were statistically weighted equally. We considered a systemic velocity difference between the primary and secondary components in HD 93249 A, shifting  $-6.9 \text{ km s}^{-1}$  the primary RVs. For ALS 12502 A, in turn, a systemic velocity difference was not detected.

To determine the orbital elements, we used the GBART (Bareilles 2017) code. It allows the user to fix the period and/or eccentricity. In this case, it was used with both parameters set to free for HD 93249 A and fixed to a circular orbit for ALS 12502 A. The results are shown in Table 3.

The new orbital solution of HD 93249 A resulted very similar to the preliminary one published by Ansín et al. (2020), except for the value of  $q$  which is slightly larger. The errors (provided by GBART) in the semi-amplitudes are smaller, indicating more accurate RV determinations. These new elements supersede those previously published. As expected, averaging three He II lines for the O-type giant and four He I lines for the B-type star provides a better representation of the binary motion of each component than a single absorption line.

The orbital solution of ALS 12502 A, unluckily, evidences an imbalance of data during quadratures (there are only two measurements in one quadrature, while there are ten in the other), this fact has no consequences on the obtained parameters because the orbit is circular (as confirmed by the photometric analysis below). Both components resulted with similar masses, i.e. their mass relation is  $q = 0.99$ . The results are shown in Table 3.

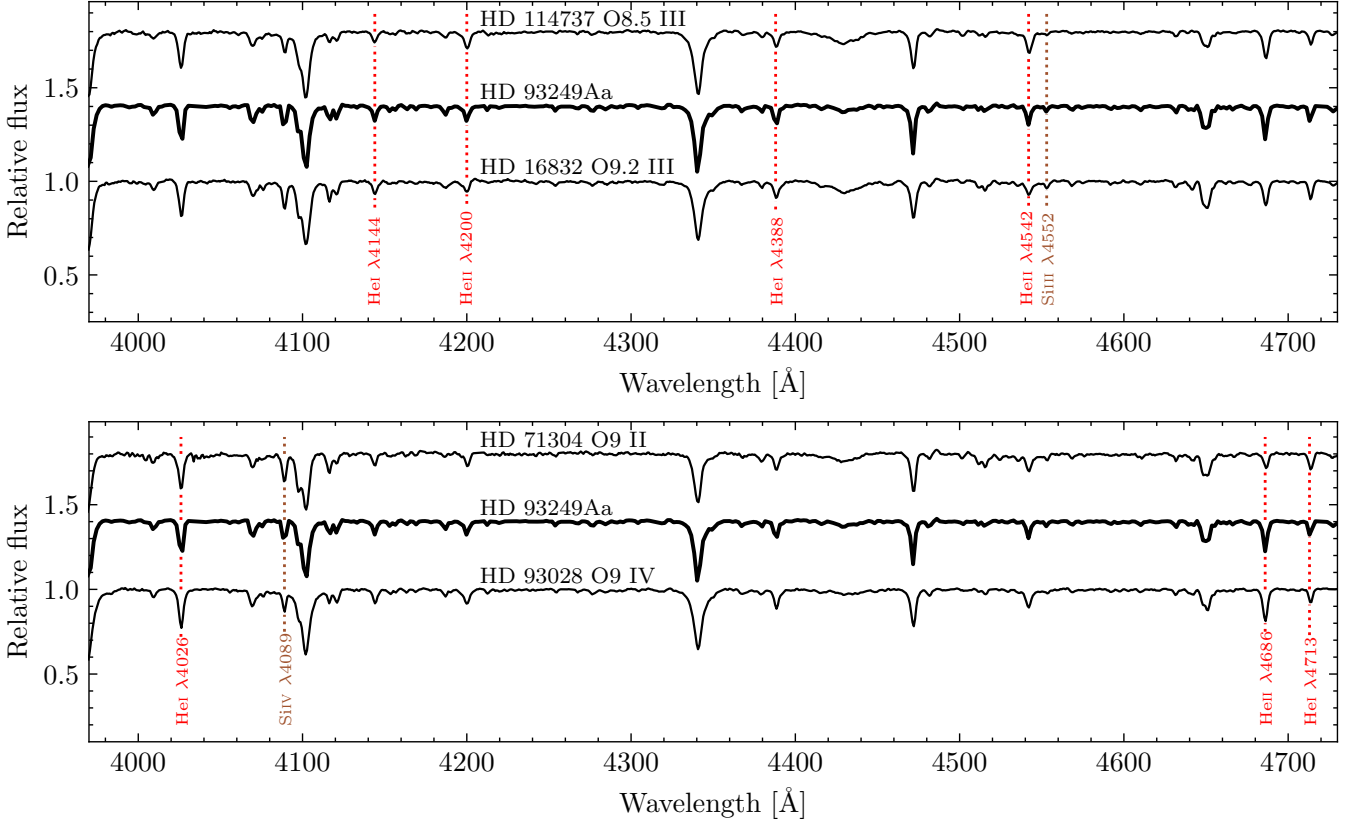


**Figure 3.** The optical spectrum of HD 93249 Aa, compared to the standards HD 114737 and HD 16832 (top) and HD 71304 and HD 93028 (bottom).

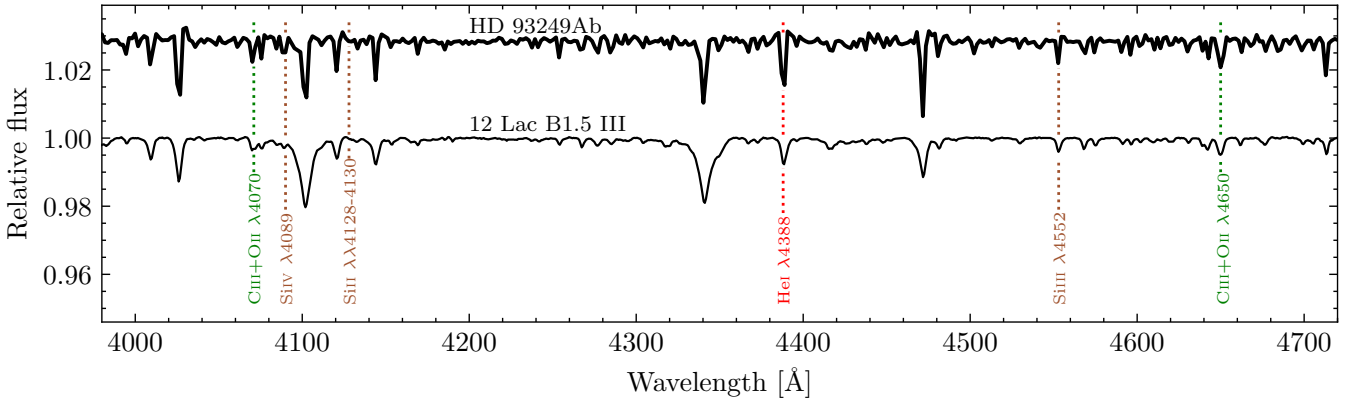


**Figure 4.** The optical spectrum of HD 93249 Ab, compared to HD 74 575 (B1.5 III).

### 3.3 TESS light curves

The very low minimum masses of both components in HD 93249 A, 0.50 and 0.24  $M_{\odot}$ , respectively (see Table 3), indicate an orbital inclination close to the celestial plane. However, we decided to analyse the extremely accurate *TESS* light curve (LC) searching for pulsations evidence or (at least) to constrain the inclination. Fig. 6 shows the LC constructed as explained in Sec. 2.2. Fig. 6 clearly presents photometric variations up to 0.005 mag. We searched the data for periodicities employing an algorithm based on the Lomb-Scargle method (Scargle 1982) implemented within the PYTHON enviroment.

The most probable period is half of the spectroscopic one meaning that the photometric variations are related to the binary orbit (see Fig. 8). Other periods found by the algorithm, and exceeding the calculated false alarm probability, resulted with a power at least three times lower than the spectroscopic one. The *TESS* data, phased with the spectroscopic period, mimic ellipsoidal variations, i.e. the subtle variations (about 0.01 mag) are modulated by the distortion of a star due to gravitational effects of its companion. The light maxima and minima coincide with quadrature and conjunction phases, respectively.

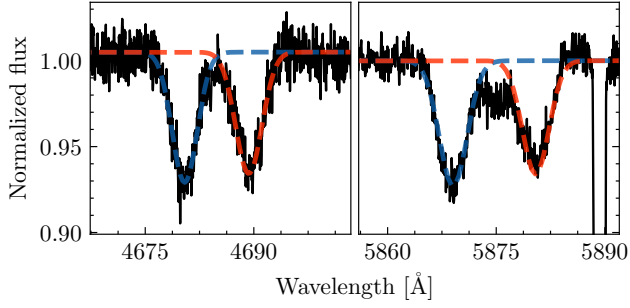


**Figure 5.** FIES spectrum of ALS 12502 A obtained at quadrature, with the best fitting of two measured lines.

**Table 3.** Orbital elements of HD 93249 A and ALS 12502 A as obtained with the GBART code.

Parameter [unit]	HD 93249 A		ALS 12502 A	
	Aa	Ab	Aa	Ab
$P$ [d]	$2.979\,68 \pm 0.000\,01$		1.95 113 (fixed)	
$T_{\text{VRmax}}$ [HJD]	$2\,454\,985.512 \pm 0.005$		$2\,456\,525.578 \pm 0.003$	
$T_0$ [HJD]	$2\,454\,985.139 \pm 0.005$		$2\,456\,524.932 \pm 0.003$	
$e$	$0.013 \pm 0.008$		0.0 (fixed)	
$\omega$ [ $^\circ$ ]	$314 \pm 33$		90	
$q$ [ $M_{\text{b}}/M_{\text{a}}$ ]	$0.483 \pm 0.009$		$0.99 \pm 0.02$	
$V\gamma$ [ $\text{km s}^{-1}$ ]	$-0.8 \pm 0.3$	$-7.7 \pm 0.3$	$-50 \pm 2$	
$K$ [ $\text{km s}^{-1}$ ]	$43.7 \pm 0.5$	$90.4 \pm 0.8$	$284 \pm 3$	$286 \pm 3$
$a \sin i$ [ $R_{\odot}$ ]	$2.55 \pm 0.03$	$5.29 \pm 0.03$	$10.9 \pm 0.1$	$11.0 \pm 0.1$
$M \sin^3 i$ [ $M_{\odot}$ ]	$0.50 \pm 0.02$	$0.24 \pm 0.02$	$19 \pm 1$	$19 \pm 1$

The LC of ALS 12502 A, shown in Fig. 7, clearly shows eclipse-like features. The LC phased with the spectroscopic period results in a double-eclipsing system which, besides, shows light maxima at both quadratures, expected to be originated in the distortions of both stars. The Lomb-Scargle method was also applied to these data and the same spectroscopic period was found (in fact, the half of it as usual in such kind of eclipsing systems, see Fig. 8).

### 3.4 Spectrophotometric analysis

Considering that both stars present RV and LC variations, we tried to model these massive binary systems by means of the PHOEBE code (Prša 2018), which is an eclipsing binary modelling code, able to reproduce and fit LC, RV curves, and spectral line profiles of eclipsing systems.

PHOEBE requires some atmospheric parameters such as bolometric albedo, gravity and limb darkening laws. We fixed the bolometric albedo and gravity to unity,  $\alpha = \beta = 1$ , according to Claret (2003). Regarding the limb darkening, we assumed a root squared law and the coefficients were taken from van Hamme (1993) and Claret (2017). We also assumed synchronous rotation for both components.

In a first attempt, we run the Nelder-Mead optimiser method, choosing the parameters to be optimised from the RV and LC separately. As expected, the orbital parameters resulted similar to those obtained with GBART and the parameters resulting from the LC fitting were used as input to the next stage, the Markov chain Monte Carlo (*emcee*; Foreman-Mackey et al. 2013) sampler within the PHOEBE 2.3 environment.

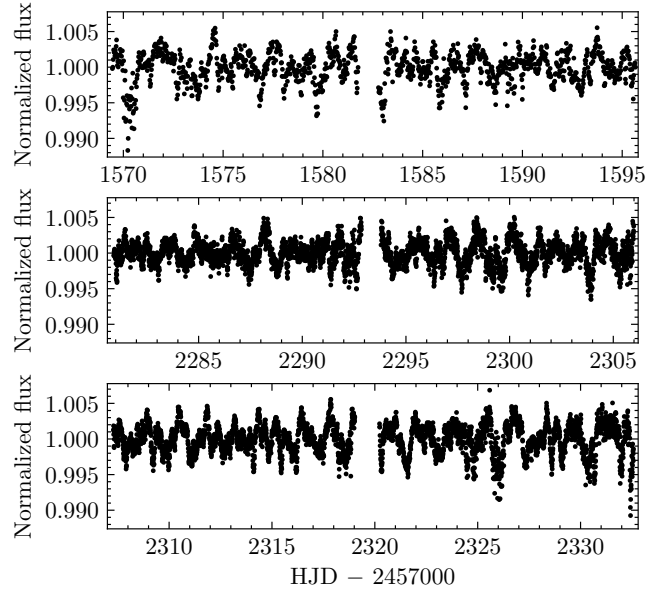


**Figure 6.** TESS light curve of HD 93249 A.

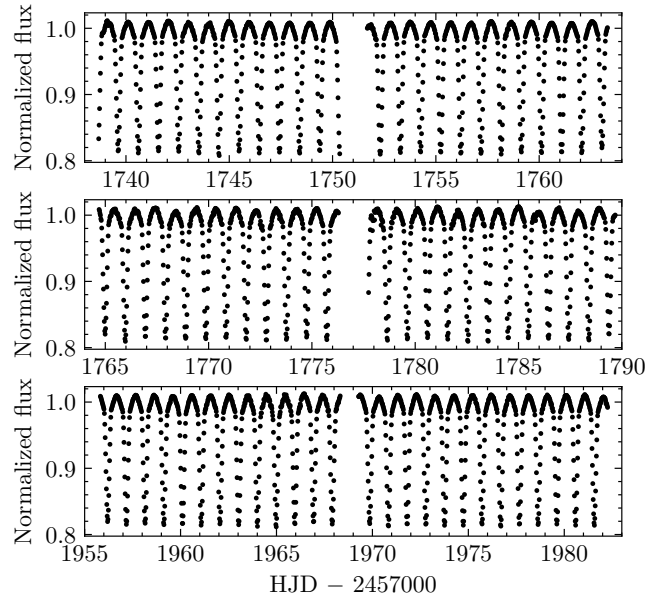


**Figure 7.** TESS light curve of ALS 12502 A.

We run *emcee* employing 24 *walkers* to explore the parameter space. For HD 93249 A we chose:  $i$ ,  $M_{\text{Ab}}$ ,  $(R_{\text{Aa}} + R_{\text{Ab}})/a$ ,  $R_{\text{Aa}}/R_{\text{Ab}}$ ,  $T_{\text{eff}}^{\text{Ab}}/T_{\text{eff}}^{\text{Aa}}$  and  $L_{\text{pb}}$  (passband luminosity), with Gaussian distributions around the optimized values of 0.5 for the inclination and mass, 0.1 for radius related parameters, 2 000 K for temperature ratio and 0.05 W for the passband luminosity. After 1500 iterations all parameters showed stable so we let take another 4000 iterations.

For ALS 12502 A we explored the parameters:  $a$ ,  $q$ ,  $i$ ,  $R_{\text{Aa}}$ ,  $R_{\text{Ab}}$  and  $L_{\text{pb}}$ , again with Gaussian distributions around the optimized values of 2, 0.5, 3, 0.5, 0.5, 0.1 for semi major axis,  $q$ , inclination, radii and luminosity. With 1000 iterations all parameters showed stable so we let take another 3000 iterations.

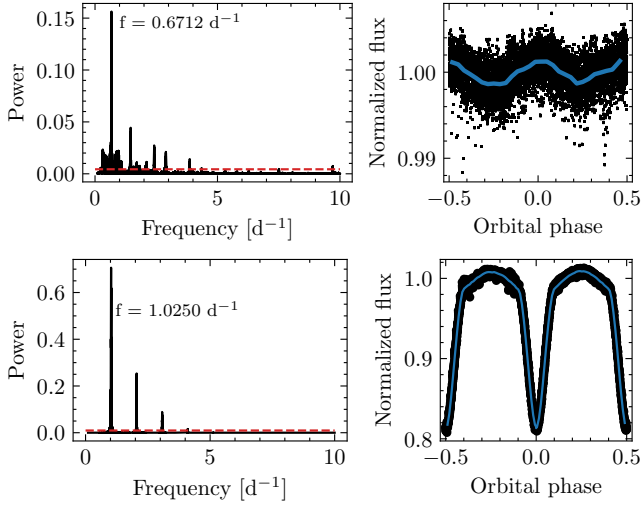


**Figure 8.** Left: Lomb-Scargle periodogram of the TESS observations of HD 93249 A and ALS 12502 A. The dashed line shows the periodogram level corresponding to a maximum peak false alarm probability of 1%. Right: Light-curve folded with twice of the first period. Binned data are plot in blue.

**Table 4.** Elements of the binary model constructed with PHOEBE for HD 93249 A.

Parameter [unit]	Aa	Ab
$i$ [°]		$16.5^{+1.9}_{-1.4}$
$a$ [ $R_{\odot}$ ]		$28.0^{+2.4}_{-2.8}$
$T_{\text{eff}}$ [K]	32 900 (fixed)	$29\,000^{+1760}_{-1600}$
$R$ [ $R_{\odot}$ ]	$9.3^{+1.2}_{-1.6}$	$4.77^{+1.51}_{-0.97}$
$M$ [ $M_{\odot}$ ]	$22.1^{+6.2}_{-5.9}$	$10.9^{+3.0}_{-2.9}$
$\log g$ [ $\text{cm s}^{-2}$ ]	$3.84^{+0.05}_{-0.03}$	$4.12^{+0.15}_{-0.14}$
$\log(L)$ [ $L_{\odot}$ ]	$5.0^{+0.1}_{-0.1}$	$4.1^{+0.4}_{-0.4}$
$M_V$	$-4.52^{+0.53}_{-0.53}$	$-2.88^{+0.92}_{-0.92}$
Observational parameters		
$m_V$	8.57	10.20
$M_V$	-4.72	-3.09
$\log(L)$ [ $L_{\odot}$ ]	5.04	4.22
Spectral Type	O9 III	B1.5 III

Errors were estimated considering  $2\sigma$  in the distribution of each parameter.

The final parameters modelling the RV and LC of both binary systems are shown in Tables 4 and 5 and illustrated in Figs. 9 and 10.

The LC of ALS 12502 A is also available in the *Gaia* DR3 database. The contribution of ALS 12502 B is expected to be negligible, then the same solution should be fit to the data, just fixing the third light to zero. In Fig. 11 it is shown the *Gaia* LC with the PHOEBE model. The agreement is good, confirming that the considerations to the third light are right.

**Table 5.** Elements of the binary model constructed with PHOEBE for ALS 12502 A.

Parameter [unit]	Aa	Ab
$i$ [°]		$73.3^{+0.1}_{-0.1}$
$a$ [ $R_{\odot}$ ]		$22.7^{+0.3}_{-0.6}$
$T_{\text{eff}}$ [K]	35 000 (fixed)	35 000 (fixed)
$R$ [ $R_{\odot}$ ]	$6.64^{+0.07}_{-0.07}$	$6.62^{+0.07}_{-0.06}$
$M$ [ $M_{\odot}$ ]	$20.84^{+0.8}_{-0.6}$	$20.6^{+0.6}_{-0.5}$
$\log g$ [ $\text{cm s}^{-2}$ ]	$4.112^{+0.006}_{-0.004}$	$4.110^{+0.004}_{-0.003}$
$\log(L)$ [ $L_{\odot}$ ]	$4.79^{+0.04}_{-0.04}$	$4.79^{+0.04}_{-0.04}$
$M_V$	$-3.9^{+0.1}_{-0.1}$	$-3.9^{+0.1}_{-0.1}$
Observational parameters		
$m_V$	10.89	10.89
$M_V$	-4.46	-4.46
$\log(L)$ [ $L_{\odot}$ ]	5.00	5.00
Spectral Type	O9 IV(n)	O9 V(n)

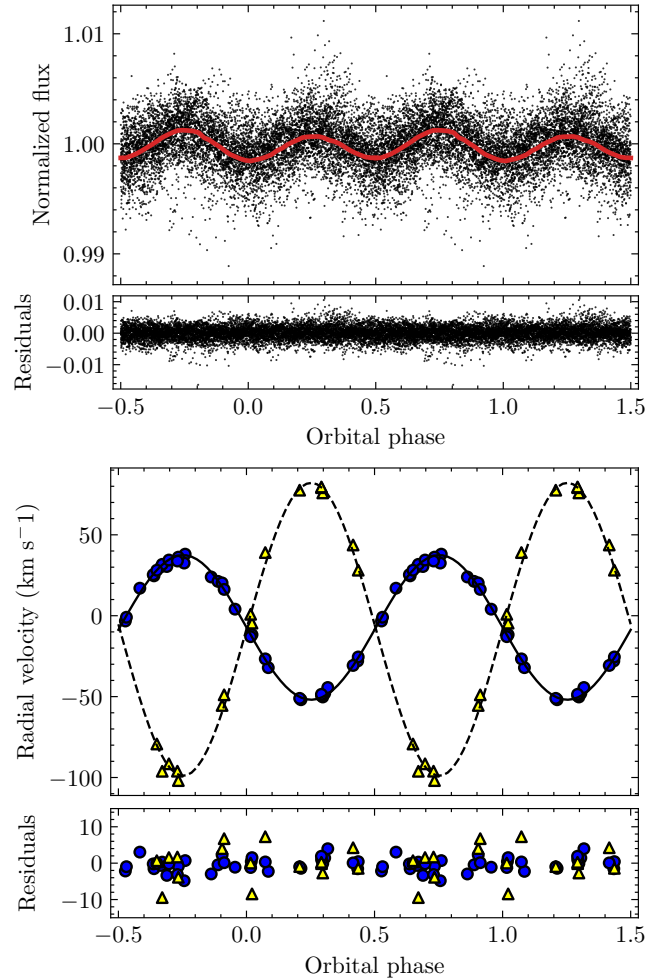


**Figure 9.** The PHOEBE model of HD 93249 A compared to the observational data.

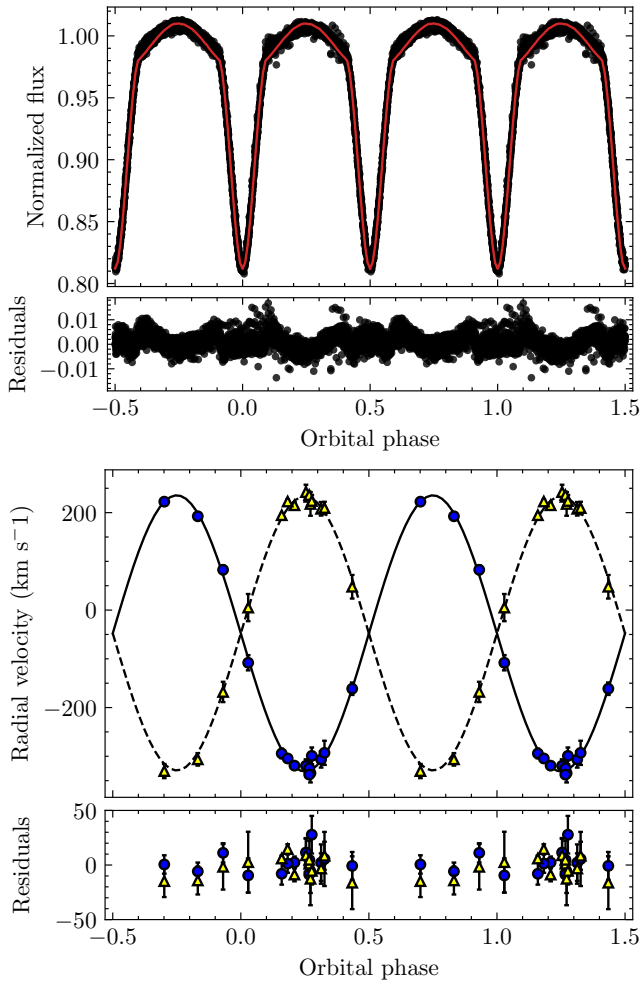


**Figure 10.** The PHOEBE model of ALS 12502 A compared to the observational data.

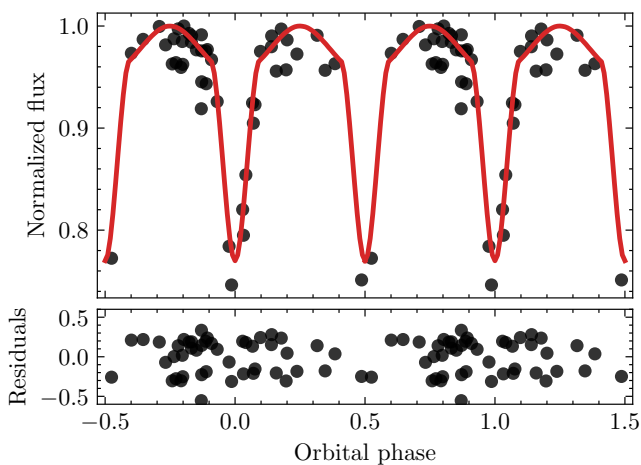


**Figure 11.** *Gaia* RP passband light curve of ALS 12502 A. The red curve represents the PHOEBE model.

**Table 6.** Spectroscopic parameters for HD 93249 A. Using IACOB-BROAD and IACOB-GBAT and assuming the observational  $M_V$  shown in Table 4.

Parameter [unit]	Aa	Ab
$v \sin i$ [km s $^{-1}$ ]	$58 \pm 6$	$16 \pm 2$
$v_{\text{mac}}$ [km s $^{-1}$ ]	$70 \pm 7$	$26 \pm 3$
$T_{\text{eff}}$ [K]	$32\,900 \pm 500$	
$\log g$ [cm s $^{-2}$ ]	3.8 (fixed)	
$R$ [ $R_{\odot}$ ]	$9 \pm 0.1$	
$M$ [ $M_{\odot}$ ]	$23 \pm 1.5$	

**Table 7.** Spectroscopic parameters for both components in ALS 12502 A. Using an ad-hoc method (see main text).

Parameter [unit]	Using	
	$\log g = 3.9$	$\log g = 4.1$
$v \sin i$ [km s $^{-1}$ ]	$200 \pm 20$	
$T_{\text{eff}}$ [K]	35 000	
$R$ [ $R_{\odot}$ ]	$8.64 \pm 1.19$	$8.65 \pm 1.2$
$M$ [ $M_{\odot}$ ]	$21.64 \pm 7.8$	$34.4 \pm 12.4$

## 4 SPECTROSCOPIC AND FUNDAMENTAL STELLAR PARAMETERS

### 4.1 Spectroscopic parameters

Following a similar technique as that described in [Holgado et al. \(2018\)](#), we applied the IACOB Grid-Based Automatic Tool (IACOB-GBAT; [Simón-Díaz et al. 2011b](#)) to the disentangled spectra of HD 93249 A to obtain estimations for the spectroscopic parameters of the stars in the system, such as effective temperatures ( $T_{\text{eff}}$ ), stellar surface gravities ( $\log g$ ), among others. IACOB-GBAT was successfully applied to the primary template but the secondary template implies cooler temperatures that are beyond the considered range of  $T_{\text{eff}}$  values of the FASTWIND grid used by this code. For the primary, we obtained the same results that [Holgado et al. \(2018\)](#) found from the composite spectrum, confirming the marginal contribution of the secondary star (See Table 6).

The case of ALS 12502 A is substantially different. We did not perform the disentangling method to its spectra, hence to derive the spectroscopic parameters from both components we decided to follow a similar strategy as that considered in [Simón-Díaz et al. \(2015b\)](#) for the case of the  $\sigma$  Ori AbAbB triple system. In brief, we tried directly to combine two FASTWIND-generated spectra, Doppler-shifted, and diluted (according to their respective fluxes), and compare them with our best composite spectrum. We calculated two solutions. One considering the surface gravity derived from PHOEBE ( $\log g = 4.1$ ) and the other with  $\log g = 3.9$ , which fits better the wings of the Balmer lines (see Table 7). In Fig. 12 we show the comparison between the best FASTWIND models and a composite spectrum.

Regarding the surface gravity for HD 93249 Aa, the IACOB-GBAT determination,  $\log g = 3.5 \pm 0.05$  dex, resulted smaller than the PHOEBE one,  $\log g = 3.84$ . The former implies adjusting models to the wings of the Balmer absorptions, which in turn, could be affected by the normalization of the échelle spectra and also (as for HD 93249 A) by the disentangling method. A discussion about this discrepancy is out of the scope of this work.

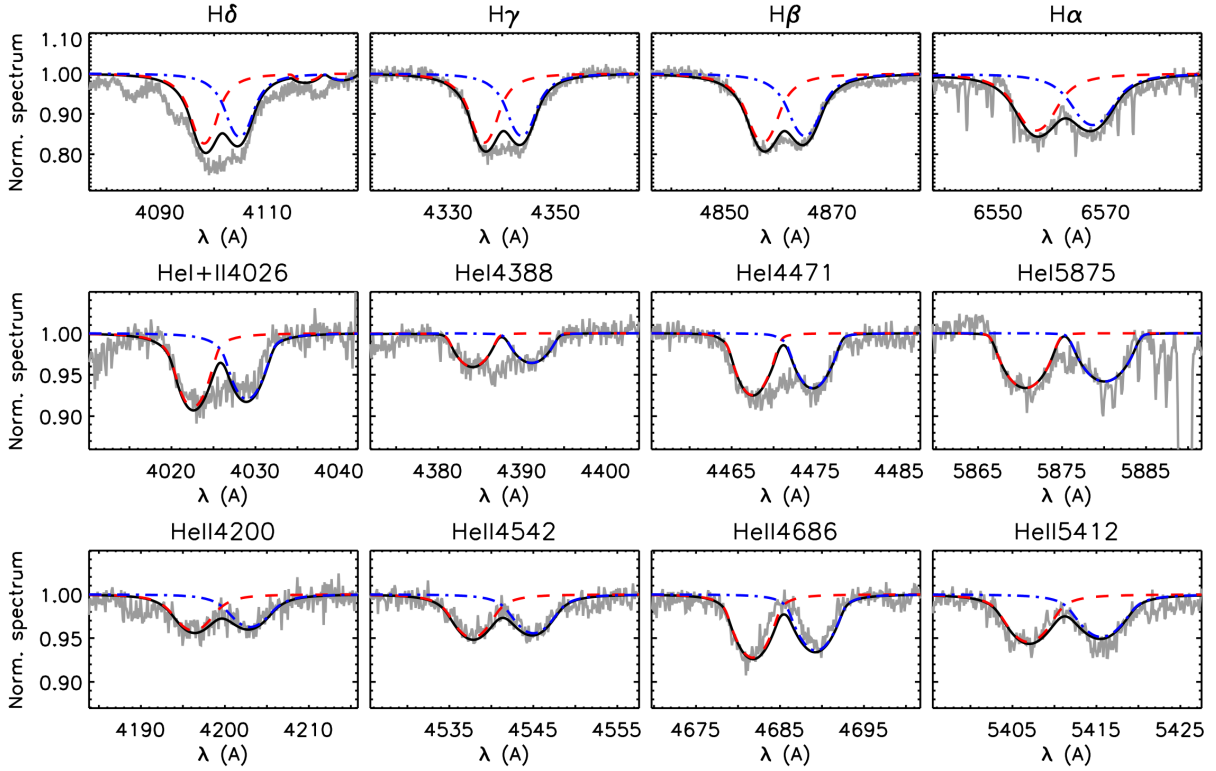


**Figure 12.** Best FASTWINDS models compared with a composite spectrum of ALS 12502 A. Blue and red lines depict the individual models (considering  $\log g = 3.9$ ) and the black one is the sum of both.

## 4.2 Fundamental parameters

Knowing radii and effective temperatures allow us to determine luminosities by the direct method using the Stefan-Boltzmann law ( $L = 4\pi R^2 \sigma T_{\text{eff}}^4$ ); those are shown in Table 4 and Table 5. We will compare these values with the luminosities calculated from the observational parameters, i.e. using the relation among distance, interstellar absorption, magnitudes, and bolometric correction ( $BC$ ).

We assumed distances from the Villafranca results (see appendix B), and extinctions from the CHORIZOS runs (see appendix C). For the absolute magnitudes and  $BC$  we used calibrations by Martins et al. (2005) and Nieva & Przybilla (2014).

As the observed  $V$  corresponds to the overall flux of the system we should express the individual magnitudes in terms of the flux ratio:

$$V_a = V + 2.5 \log \left( 1 + \frac{F_b}{F_a} \right) \quad (1)$$

$$V_b = V + 2.5 \log \left( 1 + \frac{F_a}{F_b} \right) \quad (2)$$

where subscripts,  $a$  and  $b$ , indicate the component in the binary system, and their flux ratio can be expressed as:

$$\frac{F_b}{F_a} = 10^{\left( \frac{M_b - M_a}{-2.5} \right)} \quad (3)$$

To calculate the flux ratio, we followed two paths. The first one considers the results of Sec. 3.4, i.e. it uses the luminosities computed with PHOEBE to derive the individual magnitudes, hence  $M_a$  and  $M_b$  came from:

$$M_{a,b} = -2.5 \log \left( \frac{L_{a,b}}{L_\odot} \right) + 4.74 - BC_{a,b} \quad (4)$$

and the  $BC_V$  for each component is computed from its  $T_{\text{eff}}$  following Martins et al. (2005). The second method consists in applying the absolute magnitude calibrations for each component provided in the literature, i.e. Martins et al. (2005) for the O-type, and Nieva & Przybilla (2014) for the B star.

Once the flux ratio is calculated, “observational” luminosities are determined. The individual magnitudes and luminosities are shown in Table 4.

In order to calculate the “observational” luminosities for both components in ALS 12502 A, we used the  $V$  magnitude predicted by CHORIZOS run,  $V = 10.14$  mag (see appendix C), and considering that both components have equal fluxes, a  $V$  magnitude of 10.89 mag is obtained for each one.

Putting all together, we obtained  $\log L = -4.9$ , which considering the uncertainties involved in the calculus it is in very good agreement with the theoretical one. Therefore, luminosities determined from observational quantities are in excellent agreement with the derived from the Stefan-Boltzmann equation, i.e. with radii and effective temperatures.

Adopting the derived luminosities, surface gravities, and effective temperatures, we put both pairs in a spectroscopic HRD and compared them with evolutionary tracks and isochrones from non-rotating, solar metallicity models (Ekström et al. 2012; Yusof et al. 2022). The HD 93249 A components are compatible with a 5 Ma age, and the ALS 12502 A, with 3 Ma, as depicted in Fig. 13. The evolutionary masses can be derived from those HRDs, then 22–24  $M_\odot$  and 13–14  $M_\odot$  resulted for the primary and secondary components in HD 93249 A, and almost 22  $M_\odot$  for both components in ALS 12502 A. Except for the spectroscopic masses for ALS 12502 A, using the surface gravity given by PHOEBE, there is a

good agreement among the evolutionary, spectroscopic and dynamical masses.

The discrepancy in the spectroscopic mass of ALS 12502 A is due to the use of the absolute magnitude,  $M_V = -4.46$  mag, as input to the IACOB-GBAT code. This algorithm calculates the stellar radius using the formula outlined in Kudritzki (1980) and derives the mass via Newton's gravitational equation, using the surface gravity ( $\log g$ ). Since the radius calculated by this method exceeds that derived from the PHOEBE model, the spectroscopic mass calculated using the higher value of  $\log g$  ( $\log g = 4.1$ ) turns out to be considerably larger than alternative calculations.

## 5 SUMMARY AND FINAL REMARKS

We applied a disentangling method to our high resolution optical spectra of HD 93249 A, obtaining individual spectra of the primary and secondary components which we classified as O9 III and B1.5 III, respectively. Although the contribution of the secondary to the composite spectrum is marginal, HD 93249 A can no longer be considered the classification standard for the O9 III type. We measured RVs for each component and determined the orbital parameters by means of the GBART code, which proved that HD 93249 A is a massive SB2 with a short period and an almost circular orbit.

We also analysed the available TESS data of HD 93249 A. We constructed its light curve identifying geometric light variations due to the non-spherical shape of the binary components. We then constructed a binary model to reproduce the RV and light variations using the *emcee* sampler in the PHOEBE environment. We obtained a reliable solution which is shown in Table 4 and depicted in Fig. 9.

We measured the RVs in our high resolution optical spectra of ALS 12502 A and obtained the SB2 orbit for the first time. Together with the TESS LC, we constructed a binary model to obtain the stellar parameters of both components in the system.

We determined the absolute dynamical masses of two O9 stars,  $22.1 \pm 6.2 M_\odot$  and  $20.6 \pm 0.6 M_\odot$ , for the giant component in HD 93249 A and the subgiant in ALS 12502 A respectively. In turn, the radii resulted  $9.3 \pm 1.6 R_\odot$  and  $6.6 \pm 0.1 R_\odot$ .

Considering that no other O9 III stars are known to be members of binary systems (see Sect. 1), the masses and radii determined should be compared with theoretical expectations. Regarding masses, the agreement is really good: a mass of  $22.04 M_\odot$  is calculated in the calibration of Martins et al. (2005, table 5). Our determined radii, instead, are smaller than expected. Something similar was found by Pablo et al. (2017) for other binary system.  $\iota$  Ori is a well-studied massive binary consisting of an O8.5 III and a B2: IV, i.e. quite similar to HD 93249 A, except for the wider ( $P = 29.133$  d) and more eccentric ( $e = 0.7452$ ) orbit. They determined masses of  $23.18 M_\odot$  and  $13.44 M_\odot$ , for the primary and secondary components, respectively, and radii of  $9.1 R_\odot$  and  $4.94 R_\odot$ , respectively; which are similar to the values found here for HD 93249 A. The stars in  $\iota$  Ori are as close as the components of HD 93249 A ( $33.7 R_\odot$  vs.  $28.5 R_\odot$ ) during periastron passage. This striking similarity should be explored in further works.

## ACKNOWLEDGEMENTS

The beginnings of this work were carried out while TA was student fellow of the Consejo Interuniversitario Nacional (CIN), Argentina. TA and RG acknowledge support from grant PICT 2019-0344. This research made use of Lightkurve, a Python package for

Kepler and TESS data analysis (Lightkurve Collaboration, 2018). J. M. A. acknowledges support from the Spanish Government Ministerio de Ciencia e Innovación and Agencia Estatal de Investigación (10.13039/501100011033) through grant PGC2018-095 049-B-C22 and from the Consejo Superior de Investigaciones Científicas through grant 2022AEP005. J. I. A. acknowledges the financial support of DIDULS/ULS, through the project PR2324063.

## DATA AVAILABILITY

This paper is based on public data of the TESS and Gaia missions, and spectroscopic data belonging to the OWN Survey and MONOS teams, available on reasonable request to Roberto Gamén or Jesús Maíz Apellániz.

## REFERENCES

- Ansín T., Gamén R., Morrell N. I., Barbá R., 2020, Boletín de la Asociación Argentina de Astronomía La Plata Argentina, **61B**, 78
- Astropy Collaboration et al., 2013, *A&A*, **558**, A33
- Astropy Collaboration et al., 2018, *AJ*, **156**, 123
- Bailer-Jones C. A. L., Rybizki J., Fousneau M., Demleitner M., Andrae R., 2021, *AJ*, **161**, 147
- Barbá R. H., Gamén R., Arias J. I., Morrell N. I., 2017, in Eldridge J. J., Bray J. C., McClelland L. A. S., Xiao L., eds, IAU Symposium Vol. 329, The Lives and Death-Throes of Massive Stars. pp 89–96, doi:10.1017/S1743921317003258
- Barbá R. H., et al., 2020, *MNRAS*, **494**, 3937
- Bareilles F., 2017, GBART: Determination of the orbital elements of spectroscopic binaries (ascl:1710.014)
- Berlanas S. R., et al., 2023, *A&A*, **671**, A20
- Brasseur C. E., Phillip C., Fleming S. W., Mullally S. E., White R. L., 2019, Astrocut: Tools for creating cutouts of TESS images (ascl:1905.007)
- Cantat-Gaudin T., Brandt T. D., 2021, *A&A*, **649**, A124
- Castelli F., Kurucz R. L., 2003, in Modelling of Stellar Atmospheres. p. 20
- Claret A., 2003, *A&A*, **406**, 623
- Claret A., 2017, *A&A*, **600**, A30
- Eker Z., et al., 2015, *AJ*, **149**, 131
- Ekström S., et al., 2012, *A&A*, **537**, A146
- Foreman-Mackey D., Hogg D. W., Lang D., Goodman J., 2013, *PASP*, **125**, 306
- Gamén R., Barbá R. H., Morrell N. I., Arias J., Maíz Apellániz J., 2008, in Revista Mexicana de Astronomía y Astrofísica Conference Series. pp 54–54
- Gamén R., et al., 2015, *A&A*, **584**, A7
- Ginsburg A., et al., 2019, *AJ*, **157**, 98
- González J. F., Levato H., 2006, *A&A*, **448**, 283
- Holgado G., et al., 2018, *A&A*, **613**, A65
- Kudritzki R. P., 1980, *A&A*, **85**, 174
- Lanz T., Hubeny I., 2003, *ApJS*, **146**, 417
- Lightkurve Collaboration et al., 2018, Lightkurve: Kepler and TESS time series analysis in Python, Astrophysics Source Code Library (ascl:1812.013)
- Lindgren L., et al., 2018, [http://www.cosmos.esa.int/documents/29201/1770596/Lindgren\\_GaiaDR2\\_Astrometry\\_extended.pdf](http://www.cosmos.esa.int/documents/29201/1770596/Lindgren_GaiaDR2_Astrometry_extended.pdf),
- Lindgren L., et al., 2021a, *A&A*, **649**, A2
- Lindgren L., et al., 2021b, *A&A*, **649**, A4
- Lutz T. E., Kelker D. H., 1973, *PASP*, **85**, 573
- Maciejewski G., Czart K., Niedzielski A., 2004, Information Bulletin on Variable Stars, **5518**, 1
- Maíz Apellániz J., 2001, *AJ*, **121**, 2737
- Maíz Apellániz J., 2004, *PASP*, **116**, 859
- Maíz Apellániz J., 2005, in Turon C., O'Flaherty K. S., Perryman M. A. C., eds, ESA Special Publication Vol. 576, The Three-Dimensional Universe with Gaia. p. 179

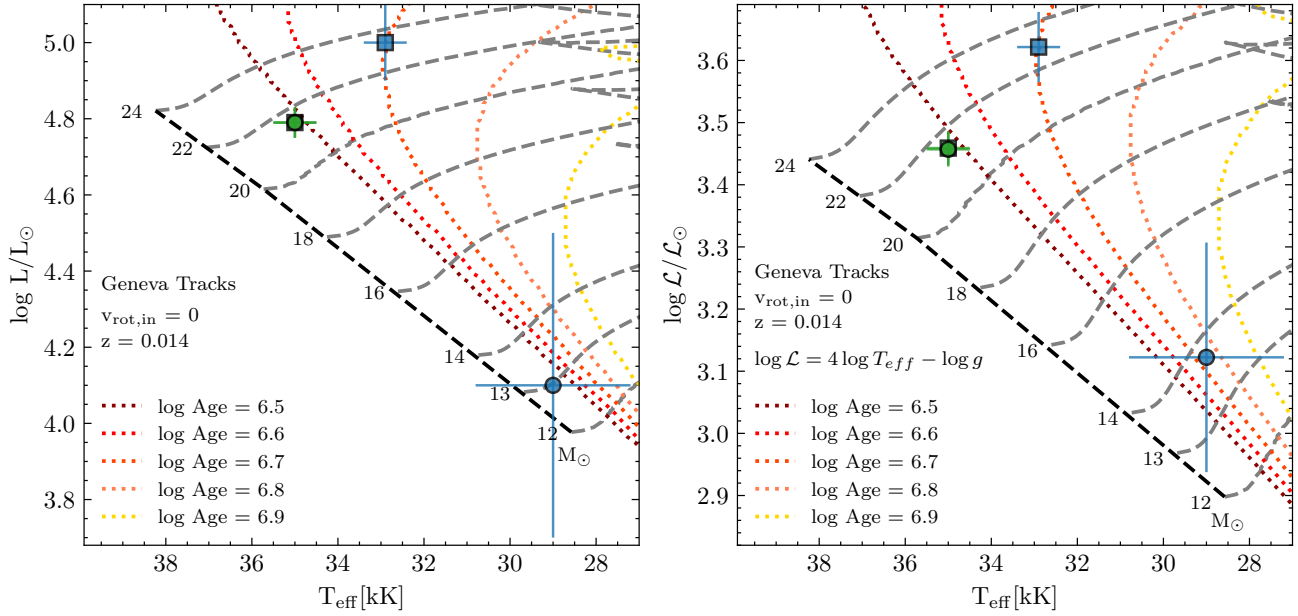


**Figure 13.** Position of the four components in the theoretical and spectroscopic HR diagrams. Blue symbols represent HD 93249 A and green, both components in ALS 12502 A superposed. Squares are the primary component and circles for secondaries. Evolutionary tracks and isochrones from non-rotating, solar metallicity models by Ekström et al. (2012) are included for reference.

Maíz Apellániz J., 2013a, in HSA 7. pp 583–589 ([arXiv:1209.2560](https://arxiv.org/abs/1209.2560))

Maíz Apellániz J., 2013b, in HSA 7. p. 657 ([arXiv:1209.1709](https://arxiv.org/abs/1209.1709))

Maíz Apellániz J., 2019, *A&A*, **630**, A119 (Villafranca 0)

Maíz Apellániz J., 2022, *A&A*, **657**, A130

Maíz Apellániz J., Barbá R. H., 2018, *A&A*, **613**, A9

Maíz Apellániz J., Barbá R. H., 2020, *A&A*, **636**, A28

Maíz Apellániz J., Weiler M., 2018, *A&A*, **619**, A180

Maíz Apellániz J., Alfaro E. J., Sota A., 2008, [arXiv:0804.2553](https://arxiv.org/abs/0804.2553),

Maíz Apellániz J., Sota A., Walborn N. R., Alfaro E. J., Barbá R. H., Morrell N. I., Gamen R. C., Arias J. I., 2011, in HSA 6. p. 467 ([arXiv:1010.5680](https://arxiv.org/abs/1010.5680))

Maíz Apellániz J., et al., 2013, in Massive Stars: From alpha to Omega. p. 198 ([arXiv:1306.6417](https://arxiv.org/abs/1306.6417))

Maíz Apellániz J., et al., 2014, *A&A*, **564**, A63

Maíz Apellániz J., et al., 2016, *ApJS*, **224**, 4

Maíz Apellániz J., Trigueros Páez E., Jiménez Martínez I., Barbá R. H., Simón-Díaz S., Pellerin A., Negueruela I., Souza Leão J. R., 2019a, in HSA 10. p. 420 ([arXiv:1810.10943](https://arxiv.org/abs/1810.10943))

Maíz Apellániz J., et al., 2019b, *A&A*, **626**, A20

Maíz Apellániz J., Pantaleoni González M., Barbá R. H., García-Lario P., Noguera-Lara F., 2020a, *MNRAS*, **496**, 4951

Maíz Apellániz J., Crespo Bellido P., Barbá R. H., Fernández Aranda R., Sota A., 2020b, *A&A*, **643**, A138

Maíz Apellániz J., Barbá R. H., Caballero J. A., Bohlin R. C., Fariña C., 2021a, *MNRAS*, **501**, 2487

Maíz Apellániz J., et al., 2021b, *MNRAS*, **506**, 3138

Maíz Apellániz J., Pantaleoni González M., Barbá R. H., 2021c, *A&A*, **649**, A13

Maíz Apellániz J., Barbá R. H., Fernández Aranda R., Pantaleoni González M., Crespo Bellido P., Sota A., Alfaro E. J., 2022, *A&A*, **657**, A131

Martins F., Schaerer D., Hillier D. J., 2005, *A&A*, **436**, 1049

Negueruela I., Steele I. A., Bernabeu G., 2004, *Astronomische Nachrichten*, **325**, 749

Negueruela I., et al., 2015, in HSA 8. pp 524–529 ([arXiv:1412.5638](https://arxiv.org/abs/1412.5638))

Nieva M.-F., Przybilla N., 2014, *A&A*, **566**, A7

Pablo H., et al., 2017, *MNRAS*, **467**, 2494

Pantaleoni González M., Maíz Apellániz J., Barbá R. H., Reed B. C., 2021, *MNRAS*, **504**, 2968

Pellerin A., Maíz Apellániz J., Simón-Díaz S., Barbá R. H., 2012, in American Astronomical Society Meeting Abstracts #219. p. 224.03

Prša A., 2018, Modeling and Analysis of Eclipsing Binary Stars. 2514–3433, IOP Publishing, [doi:10.1088/978-0-7503-1287-5](https://doi.org/10.1088/978-0-7503-1287-5), <http://dx.doi.org/10.1088/978-0-7503-1287-5>

Putkuri C., Gamen R., Morrell N. I., Simón-Díaz S., Barbá R. H., Ferrero G. A., Arias J. I., Solivella G., 2018, *A&A*, **618**, A174

Putkuri C., Gamen R., Morrell N. I., Benvenuto O. G., Barbá R. H., Arias J. I., 2021, *A&A*, **650**, A96

Riello M., et al., 2021, *A&A*, **649**, A3

Scargle J. D., 1982, *ApJ*, **263**, 835

Shull J. M., Darling J., Danforth C. W., 2021, *ApJ*, **914**, 18

Simón-Díaz S., García M., Herrero A., Maíz Apellániz J., Negueruela I., 2011a, in Stellar Clusters & Associations: A RIA Workshop on Gaia. pp 255–259 ([arXiv:1109.2665](https://arxiv.org/abs/1109.2665))

Simón-Díaz S., Castro N., Herrero A., Puls J., García M., Sabín-Sanjulián C., 2011b, in Journal of Physics Conference Series. p. 012021 ([arXiv:1111.1341](https://arxiv.org/abs/1111.1341)), [doi:10.1088/1742-6596/328/1/012021](https://doi.org/10.1088/1742-6596/328/1/012021)

Simón-Díaz S., et al., 2015a, in Highlights of Spanish Astrophysics VIII. pp 576–581 ([arXiv:1504.04257](https://arxiv.org/abs/1504.04257)), [doi:10.48550/arXiv.1504.04257](https://doi.org/10.48550/arXiv.1504.04257)

Simón-Díaz S., et al., 2015b, *ApJ*, **799**, 169

Simón-Díaz S., Pérez Prieto J. A., Holgado G., de Burgos A., Iacob Team 2020, in XIV.0 Scientific Meeting (virtual) of the Spanish Astronomical Society. p. 187

Sota A., Maíz Apellániz J., Morrell N. I., Barbá R. H., Walborn N. R., Gamen R. C., Arias J. I., Alfaro E. J., 2014, *ApJS*, **211**, 10

Trigueros Páez E., Barbá R. H., Negueruela I., Maíz Apellániz J., Simón-Díaz S., Holgado G., 2021, *A&A*, **655**, A4

Walborn N. R., 1973, *ApJ*, **179**, 517

Walborn N. R., Fitzpatrick E. L., 1990, *PASP*, **102**, 379

Yusuf N., et al., 2022, *MNRAS*, **511**, 2814

van Hamme W., 1993, *AJ*, **106**, 2096

van Leeuwen F., 2007a, Hipparcos, the New Reduction of the Raw Data. Hipparcos, the New Reduction of the Raw Data. By Floor van Leeuwen, Institute of Astronomy, Cambridge University, Cambridge, UK Series: Astrophysics and Space Science Library, Vol. 350 20 Springer Dordrecht

van Leeuwen F., 2007b, *A&A*, **474**, 653

## APPENDIX A: RADIAL VELOCITIES MEASURED

In Table A1 we show the radial velocities (RVs) measured for both components of HD 93249 A, which are indicated with the subscripts "a" and "b". In successive columns we tabulate the Heliocentric Julian Day (HJD), the RVs measured applying `NGAUSS` to the He I  $\lambda 5876$  absorption line for both components, the mean RVs of the interstellar D<sub>1</sub> and D<sub>2</sub> features –for comparison purposes– labeled as IS, and the RVs determined for each component using `FXCOR` (see main text) along with their errors.

In Table A2, in turn, we tabulate the Heliocentric Julian Day (HJD), the RVs measured applying `PYTHON SCIPY` (see main text) to the He I  $\lambda 5876$  and He II  $\lambda 4686$  and  $\lambda 5412$  absorption lines for both components, and their weighted average. Errors in RVs ( $a_{\text{err}}$  and  $b_{\text{err}}$ ) were calculated converting the uncertainty in the fit of the central wavelength to velocity.

## APPENDIX B: DISTANCES

This Appendix describes how we calculate *Gaia*-based distances. First, we describe the calibration of individual parallaxes, then we describe how group parallaxes for a stellar cluster are obtained, we continue with a discussion of priors for the young Galactic stellar population (either OB stars or young stellar clusters), and we end with the results for Villafranca O-034.

### B1 *Gaia* EDR3 calibration

The *Gaia* archive provides parallaxes with internal uncertainties, not external ones. That is, the catalog uncertainties are just the result of the pipeline that generates the data but they have not been validated (i.e. externally calibrated). We do that using the general scheme of Lindegren et al. (2018), a document generated by members of the *Gaia* team in charge of astrometry. In such a procedure, systematic biases are first eliminated in as much as possible, a calibration is added for the random uncertainties, and the resulting (leftover) systematic and random uncertainties are added in quadrature, with a special treatment to deal with the angular covariance remaining in the systematic biases (an issue that is of special relevance for stellar clusters such as Villafranca O-034).

The *Gaia* EDR3 astrometric solution (note that *Gaia* DR3 did not provide new astrometry) is described in Lindegren et al. (2021a). The *Gaia* team provided a correction for the systematic parallax biases (or zero point) in Lindegren et al. (2021b) but those same authors encouraged further work by stating that “*This paper does not claim to give a definitive answer but merely a rough characterisation of what we have found to be the main dependences. It is likely that better and possibly quite different estimates can be obtained in the future by means of more refined and comprehensive analysis methods*”. They also added that “*increasing the amount of data included in a global analysis could improve the precision of the bias estimation and perhaps extend its validity in magnitude–colour space. Examples of datasets that should be explored are the stars in open and globular clusters, which have the potential to cover a wide range in magnitudes and different environments*”.

With those ideas in mind, Maíz Apellániz et al. (2021c) and Maíz Apellániz (2022) obtained a new *Gaia* EDR3 calibration based on stellar clusters, which is the one that we use here. Its most relevant characteristics are:

- A new determination of the *Gaia* EDR3 parallax bias that is

significantly different for bright stars, the parameter range less explored by Lindegren et al. (2021b) and that is relevant for the objects analysed in this paper.

- A calculation of the multiplicative correction factor to be applied for the parallax uncertainties, which happen to be significantly underestimated, especially for bright stars. This indicates that *Gaia* EDR3-based distances that assume no correction factor (to our knowledge, most published papers so far do this as they do not mention it) underestimate the uncertainties.
- A special treatment for targets with six-parameter astrometric solutions or with large values of RUWE (Lindegren et al. 2021a).
- An estimation of the angular covariance associated with *Gaia* EDR3 parallaxes. Its values are relatively high for short angles. Hence, it is very important to include its effect when calculating distances to stellar clusters, as they are usually limited by the angular covariance and not by the individual uncertainties for each star.

The calibration above does not affect proper motions. However, Cantat-Gaudin & Brandt (2021) have derived a correction for the *Gaia* EDR3 proper motions of bright stars that we also include in our analysis.

### B2 Group parallaxes and the Villafranca project

In the Villafranca project (Maíz Apellániz et al. 2020b, 2022) we are combining *Gaia* photometry, astrometry, and spectroscopy with ground-based spectroscopic surveys such as GOSSS (Maíz Apellániz et al. 2011) and LiLiMaRlin (Maíz Apellániz et al. 2019a) and the GALANTE photometric survey (Maíz Apellániz et al. 2021b). As part of the Villafranca project, the distance to HD 93249 A was determined considering it as a member of Trumpler 15 (Villafranca O-027),  $d = 2355^{+61}_{-58}$  pc (Molina-Lera et al. in preparation). A similar analysis is lacking for the underlying ALS 12502 A cluster and we produce it here, adding it to the Villafranca catalog as Villafranca O-034. In order to so, we first briefly explain the procedure used to calculate the group parallaxes for the Villafranca stellar OB groups, which was first used in Maíz Apellániz (2019), applied to the specific cluster analyzed here.

We selected the *Gaia* EDR3 stars within  $240''$  of the  $\alpha = 338.69^\circ$ ,  $\delta = +58.30^\circ$  position; within 0.30 mas/a of the proper motion  $\mu_{\alpha^*} = -3.40$  mas/a,  $\mu_{\delta} = -2.20$  mas/a;  $\Delta(G'_{\text{BP}} - G'_{\text{RP}}) > -1.00$  (selection range in the CMD referred as a colour displacement with respect to a reference isochrone, see the green lines in Fig. B1 and Maíz Apellániz et al. 2020b),  $\text{RUWE} < 1.4$  (Renormalized Unit Weight Error, a measurement of the *Gaia* EDR3 astrometric quality, see Lindegren et al. 2021a);  $C^* < 0.4$  (a measurement of the *Gaia* EDR3 photometric contamination, see Riello et al. 2021); and  $\sigma_{\text{ext}} < 0.1$  mas (the *Gaia* EDR3 external parallax uncertainty as determined from the calibration process described in the previous subsection). As for the rest of the Villafranca groups, we apply a three-sigma filtering in normalized parallax and in Table B1 we give (see Table 2 in Maíz Apellániz et al. 2022 for references):

- $N_{*,0}$ : Number of stars in group before normalized parallax filtering.
- $N_*$ : Number of stars in group after normalized parallax filtering.
- $t_{\varpi}$ : Normalized  $\chi^2$  test for the group parallax.
- $t_{\mu_{\alpha^*}}$ : Normalized  $\chi^2$  test for the group proper motion in  $\alpha$ .
- $t_{\mu_{\delta}}$ : Normalized  $\chi^2$  test for the group proper motion in  $\delta$ .
- $\varpi_g$ : Group parallax and uncertainty.
- $d$ : Distance and uncertainty (see next subsection).

We point out that the  $\varpi_g$  and  $d$  uncertainties are dominated by the

**Table A1.** Radial velocities measured for both components of HD 93249 A.

HJD 2400000+	NGAUSS			FXCOR				Telescope
	a	b	<IS>	a	a <sub>err</sub>	b	b <sub>err</sub>	
54 510.797	-23	35	4	-21.0	1.1	-	-	CAS
54 585.566	5	-41	3	3.7	0.5	-	-	CAS
54 609.572	17	-59	3	23.9	0.9	-	-	CAS
54 642.513	28	-78	4	31.6	0.4	-	-	CAS
54 644.499	-46	78	4	-41.1	1.2	-	-	CAS
54 845.797	29	-85	1	30.9	0.8	-	-	CAS
54 846.841	-48	76	2	-45.0	0.7	-	-	CAS
54 847.790	5	-35	1	6.0	0.7	-	-	CAS
54 848.855	25	-66	1	28.2	0.7	-	-	CAS
54 953.524	-13	2	6	-6.0	0.2	0.9	0.2	LS
54 955.553	37	-95	6	41.3	0.3	-91.5	0.4	LS
54 956.674	-22	38	6	-19.7	0.2	39.0	0.4	LS
54 961.622	34	-102	5	43.1	0.3	-101.9	0.8	LCO
54 962.479	-11	11	6	-4.8	0.4	-4.6	0.4	LCO
54 978.613	-22	28	6	-18.6	0.2	28.1	0.2	LS
54 982.559	42	-97	7	45.0	0.7	-	-	CAS
54 983.526	-25	49	4	-25.2	0.8	-	-	CAS
54 985.527	42	-86	6	39.5	0.4	-	-	CAS
55 606.644	-43	76	6	-44.1	0.1	77.6	0.3	LS
55 642.669	-44	84	7	-43.3	0.2	75.9	0.4	LS
55 697.592	38	-95	6	40.7	0.3	-96.1	0.3	LS
55 699.636	-26	46	6	-23.8	0.1	43.7	0.2	LS
56 067.616	18	-47	6	23.2	0.1	-48.9	0.6	LS
56 079.511	24	-54	6	27.2	0.2	-55.5	0.5	LCO
56 098.546	-45	86	6	-42.6	0.2	79.1	0.4	LS
56 120.530	37	-82	5	38.7	0.2	-96.1	0.6	LCO
57 117.595	-45	83	6	-41.6	0.2	79.6	0.3	LS
58 596.632	33	-91	3	37.2	1.0	-	-	CAS
58 597.680	-12	23	4	-5.1	0.5	-	-	CAS
58 598.570	-44	69	6	-37.4	0.6	-	-	CAS
58 599.519	28	-79	5	32.3	0.6	-	-	CAS
58 599.561	20	-84	6	35.1	0.4	-79.3	0.5	LCO
58 600.471	8	-37	5	11.0	0.8	-	-	CAS
58 632.454	-	-	-	37.3	1.3	-	-	CAS

**Table A2.** Radial velocities measured for both components of ALS 12502 A.

HJD 2 450 000+	He I $\lambda 5876$				He II $\lambda 4686$				He I $\lambda 5412$				Weighted average				<IS>	Telescope
	a	a <sub>err</sub>	b	b <sub>err</sub>	a	a <sub>err</sub>	b	b <sub>err</sub>	a	a <sub>err</sub>	b	b <sub>err</sub>	a	a <sub>err</sub>	b	b <sub>err</sub>		
56 253.440	-332	5	231	6	-363	10	174	12	-308	11	232	9	-335	19	218	24	-18	CAFE 2.2
56 264.481	76	5	-147	5	79	7	-198	8	97	8	-171	6	83	9	-168	21	-19	CAFE 2.2
56 292.341	-314	2	221	3	-323	5	203	66	-327	6	209	4	-319	5	215	6	-19	CAFE 2.2
56 522.662	-309	3	232	5	-318	6	230	8	-342	7	263	6	-319	13	242	15	-15	CAFE 2.2
56 524.639	-312	3	231	3	-320	5	226	6	-354	5	239	4	-324	18	232	5	-16	CAFE 2.2
58 303.603	-51	35	-56	39	-112	6	-13	6	-113	5	34	6	-108	16	5	28	-16	NOT
58 415.610	-148	2	21	2	-178	3	67	3	-161	4	72	5	-161	13	48	24	-16	MERCATOR
58 448.452	-335	2	230	2	-335	5	232	4	-342	2	246	3	-338	3	236	7	-16	NOT
58 450.493	-289	2	201	2	-311	5	193	5	-327	3	227	3	-306	17	208	14	-16	NOT
59 858.909	-285	2	193	3	-312	6	200	5	-299	3	194	3	-294	10	195	3	-18	GEMINI
59 884.319	-300	5	220	7	-318	8	219	8	-299	6	229	8	-304	8	223	4	-16	MERCATOR
59 885.330	211	6	-315	6	229	7	-328	9	229	7	-349	7	222	8	-330	15	-16	MERCATOR
59 890.453	-261	3	193	3	-302	4	218	4	-319	4	221	4	-293	25	209	13	-16	NOT
59 891.439	184	4	-291	4	192	4	-316	6	203	4	-318	5	193	8	-306	13	-16	NOT
59 892.307	-276	3	209	5	-307	2	241	5	-317	4	222	4	-299	17	224	12	-16	NOT

**Table B1.** Villafranca O-034 astrometric results, see the text for notation.

ID	$N_{*,0}$	$N_*$	$t_{\varpi}$	$t_{\mu_{\alpha^*}}$	$t_{\mu_{\delta}}$	$\mu_{\alpha^*,g}$ (mas/a)	$\mu_{\delta,g}$ (mas/a)	$\varpi_g$ (mas)	$d$ (pc)
O-034	37	37	1.10	2.74	2.43	$-3.355 \pm 0.024$	$-2.207 \pm 0.024$	$0.258 \pm 0.011$	$3890^{+190}_{-170}$

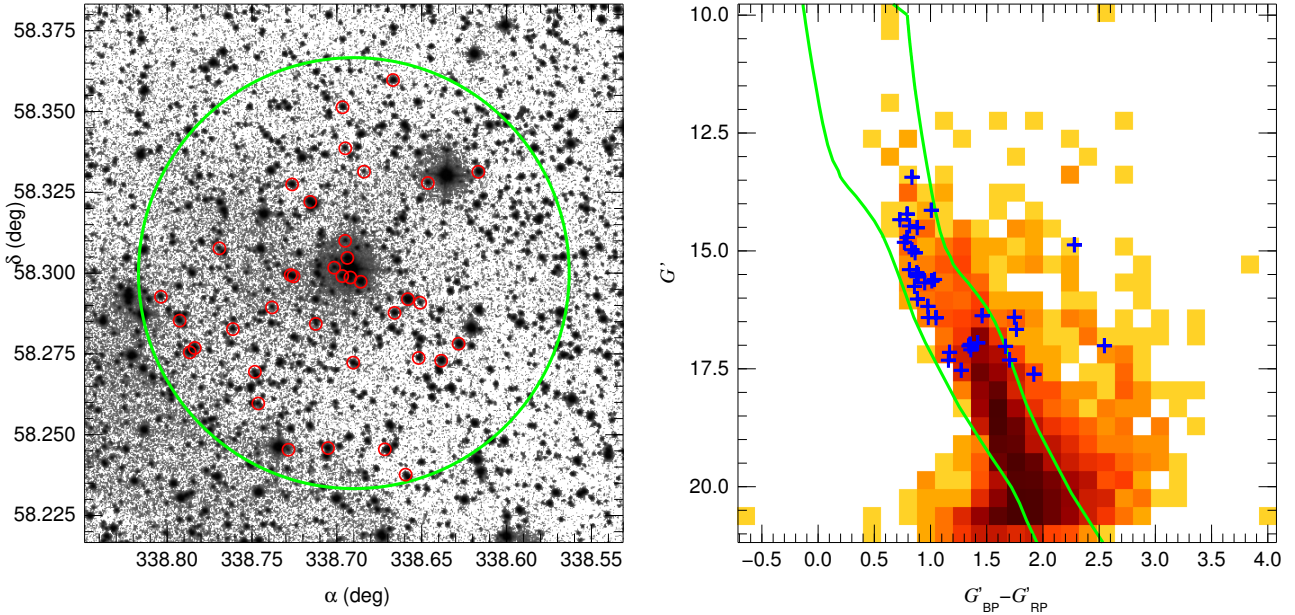


**Figure B1.** Villafranca O-034 selection results. The left panel shows the 37 selected cluster members on top of a negative DSS2 Blue image with a green circle indicating the search zone. See [Maíz Apellániz et al. \(2019b\)](#) for an AstraLux image of the central region. The right panel shows the *Gaia* EDR3 color-magnitude diagram using the same style as in the papers of the Villafranca project ([Maíz Apellániz et al. 2020b](#)), with the background giving the total source density in the region, blue crosses indicating the selected members, and the green lines showing the reference extinguished isochrone (right) and the displaced isochrone used as constraint (left), joined at the top by the extinction trajectory.

angular covariance term ([Maíz Apellániz et al. 2021c](#)), as expected, and have values of  $\sim 4.6\%$  for a distance slightly under 4 kpc. That is in line with the *Gaia* EDR3 results for the other Villafranca clusters, for which the uncertainty in percentage is approximately the distance in kpc. This is a fundamental limit of the *Gaia* EDR3 parallaxes: published cluster parallaxes with significantly lower uncertainties are likely to have been calculated without taking into account the covariance term and may be underestimated.

### B3 Priors and stellar distributions

[Lutz & Kelker \(1973\)](#) discovered half a century ago that the inversion of trigonometric parallaxes to obtain distances could be severely biased if the relative uncertainties are large and an underlying uniform spatial distribution is assumed. This issue was first addressed for the young Galactic stellar population by [Maíz Apellániz \(2001\)](#), who derived the spatial distribution of O-B5 stars in the solar neighbourhood from Hipparcos parallaxes and used it to derive improved distance estimates based on them. Later on, [Maíz Apellániz \(2005\)](#) converted the previous analysis into a Bayesian formalism with a prior that could be used for young Galactic populations in general (OB stars and young clusters and associations). [Maíz Apellániz et al. \(2008\)](#) used the improved Hipparcos calibration of [van Leeuwen \(2007a,b\)](#) to derive improved parameters for the prior. Those are

the ones that we use in this paper to calculate *Gaia* EDR3-based distances.

Why not use the [Bailer-Jones et al. \(2021\)](#) distances instead? There are two reasons, a general one and a specific one for our analysis. The general one is that [Bailer-Jones et al. \(2021\)](#) uses the [Lindgren et al. \(2021b\)](#) calibration instead of the one described above. This leads to biases, especially for bright stars. The second one is that the [Bailer-Jones et al. \(2021\)](#) prior is for the general stellar population of the Galaxy, which has a spatial distribution significantly different from that of OB stars or young stellar clusters. This leads to significant differences, especially for objects located several kpc away. See [Pantaleoni González et al. \(2021\)](#) for a comparison of *Gaia* DR2 distances obtained with different priors.

### B4 Results for Villafranca O-034

The selected cluster members and the CMD are shown in Fig. B1. The cluster is sparsely populated but with a clear concentration around ALS 12502 A. The 37 selected members form a well defined isochrone, with a few objects to the right that could be PMS stars or embedded objects. ALS 12502 A is not selected as a cluster member due to its large RUWE, as expected, and ALS 12502 B is not selected, either, in this case because of the lack of  $G_{BP}$  and  $G_{RP}$  photometry. The brightest selected member

**Table C1.** Results for the HD 93249 A and ALS 12502 A CHORIZOS runs.

	HD 93249 A	ALS 12502 A
$T_{\text{eff}}$ (kK)	32.0 (fixed)	32.0 (fixed)
LC	3.594±0.033	3.166±0.024
$R_{5495}$	3.580±0.110	3.946±0.086
$E(4405 - 5495)$ (mag)	0.398±0.007	0.608±0.010
$\log d$ (pc)	3.372 (fixed)	3.590 (fixed)
$\chi_{\text{red}}^2$	0.42	3.97
$A_G$ (mag)	1.411±0.021	2.311±0.019
$G_0$ (mag)	6.889±0.021	7.672±0.018
$L$ ( $10^5$ solar)	1.193±0.023	1.582±0.026

is 2MASS 22343797+5817310. The value of  $t_{\text{ev}}$  close to 1.0 is an indication of the reality of the cluster as a stellar group at a fixed distance.  $t_{\mu_{\alpha^*}}$  and  $t_{\mu_{\delta}}$  have values consistent with the expected internal motions (Maíz Apellániz et al. 2022).

### APPENDIX C: EXTINCTION DETERMINATION

As mentioned in the text, we did CHORIZOS (Maíz Apellániz 2004) runs to determine the extinction towards HD 93249 A and ALS 12502 A. Here we describe the details of those runs:

- We used the *Gaia* DR2 + EDR3 and 2MASS photometry (a total of nine bands) for those stars. The reason for using both *Gaia* data releases is that there are significant color terms between them, especially for  $G_{\text{BP}}$ , which can be exploited to better constrain the SED parameters. For *Gaia* DR2 we used the passbands and calibration procedure described in Maíz Apellániz & Weiler (2018) updated with the treatment developed for *Gaia* EDR3 (Weiler et al. in preparation) that includes new passband definitions with significant changes in the Balmer jump region, which is crucial for the SED analysis of O-type stars.

- As SED grid we used the solar metallicity one of Maíz Apellániz (2013b), which for O stars is built from a TLUSTY OSTAR2002 optical part (Lanz & Hubeny 2003) and an ATLAS9 NIR part (Castelli & Kurucz 2003), as the TLUSTY SEDs yield incorrect NIR colors. The two intrinsic parameters of the SED grid are effective temperature and (photometric) luminosity class, defined in an analogous way to the luminosity class used for spectral classification in the MK system but making it continuous instead of discrete, with 0.0 corresponding to hypergiants and 5.5 to the ZAMS (see Fig. 2 in Maíz Apellániz 2013b).

- We have used the family of extinction laws of Maíz Apellániz et al. (2014), whose two parameters are amount [ $E(4405 - 5495)$ ] and type [ $R_{5495}$ ] of extinction. It is important to emphasize that those are monochromatic quantities as opposed to band-integrated ones (which would be  $E(B - V)$  and  $R_V$ , respectively). Due to the non-linear effects of extinction, using band-integrated quantities to define extinction laws leads to errors and inconsistencies, especially when applied to filters with very wide passbands such as the *Gaia* ones (Maíz Apellániz 2013a; Maíz Apellániz & Barbá 2018; Maíz Apellániz et al. 2020a).

- For the sake of consistency, we applied the same procedure as in Maíz Apellániz & Barbá (2018) and Maíz Apellániz et al. (2021a), as our long-term goal (started in those papers) is to produce homogeneous extinction parameters for all of the O stars in the GOSSS project (Maíz Apellániz et al. 2011). As in those papers, we fixed  $T_{\text{eff}}$  from the spectral types and  $\log d$  from the Villafranca results. This

left us with three free parameters: luminosity class [LC], amount of extinction [ $E(4405 - 5495)$ ] and type of extinction [ $R_{5495}$ ]. Doing the runs in that way assumes that all the light is coming from a single source with the  $T_{\text{eff}}$  of the primary, that is, the resulting LC corresponds to that of the total luminosity assuming no temperature differences between the components of the binary.

Results are given in Table C1. The  $\chi_{\text{red}}^2$  for the HD 93249 A fit is excellent but that for ALS 12502 A is somewhat large. One possible origin could be a different sampling of the eclipses in the ALS 12502 A magnitudes in *Gaia* DR2 and EDR3, leading to magnitude differences between the two (the target is slightly brighter in EDR3). ALS 12502 A is significantly more extinguished than HD 93249 A and its  $R_{5495}$  is also higher. Both have (photometric) luminosity classes between 3.0 and 4.0, as expected of evolved O stars with a (spectroscopic) luminosity class of III with a hidden companion, with (the combined) ALS 12502 A being somewhat more luminous than (the combined) HD 93249 A. Results are shown in Table C1.

ALS 12502 A was not included in the Maíz Apellániz & Barbá (2018) sample but HD 93249 A was. If we compare the result for HD 93249 A for  $R_{5495}$  and  $E(4405 - 5495)$  with the new one (adding the uncertainties in quadrature), we find a good agreement with a difference of only  $\sim 1$  sigma, with the new values being more precise. This is a good test of the robustness of the CHORIZOS runs, as the photometry in the two papers is different, with only the 2MASS magnitudes in common.

This paper has been typeset from a  $\text{\LaTeX}$  file prepared by the author.